HHS Public Access

Author manuscript

Cytokine. Author manuscript; available in PMC 2023 August 30.

Published in final edited form as:

Cytokine. 2022 November ; 159: 155972. doi:10.1016/j.cyto.2022.155972.

Exogenous Oncostatin M Induces Cardiac Dysfunction, Musculoskeletal Atrophy, and Fibrosis

Daenique H.A. Jengelley[1,7], **Meijing Wang**[2,7], **Ashok Narasimhan**[2,7], **Joseph E. Rupert**[1,7], **Andrew R. Young**[2], **Xiaoling Zhong**[2,6,7], **Daniel J. Horan**[3,7], **Alexander G. Robling**[3,5,7], **Leonidas G. Koniaris**[2,3,5,6,7], **Teresa A. Zimmers**[1,2,3,4,5,6,7]

[1]Department of Biochemistry and Molecular Biology, Indiana University School of Medicine

[2]Department of Surgery, Indiana University School of Medicine

[3]Department of Anatomy, Cell Biology & Physiology, Indiana University School of Medicine

[4]Department of Otolaryngology—Head & Neck Surgery, Indiana University School of Medicine

[5]Indiana Center for Musculoskeletal Health

[6]Indiana University Melvin and Bren Simon Comprehensive Cancer Center

[7]Richard L. Roudebush Veterans Administration Medical Center, Indianapolis, IN 46202, USA

Abstract

Musculoskeletal diseases such as muscular dystrophy, cachexia, osteoarthritis, and rheumatoid arthritis impair overall physical health and reduce survival. Patients suffer from pain, dysfunction, and dysmobility due to inflammation and fibrosis in bones, muscles, and joints, both locally and systemically. The Interleukin-6 (IL-6) family of cytokines, most notably IL-6, is implicated in musculoskeletal disorders and cachexia. Here we show elevated circulating levels of OSM in murine pancreatic cancer cachexia and evaluate the effects of the IL-6 family member, Oncostatin M (OSM), on muscle and bone using adeno-associated virus (AAV) mediated over-expression of murine OSM in wildtype and IL-6 deficient mice. Initial studies with high titer AAV-OSM injection yielded high circulating OSM and IL-6, thrombocytosis, inflammation, and 60% mortality without muscle loss within 4 days. Subsequently, to mimic OSM levels in cachexia, a lower titer of AAV-OSM was used in wildtype and *Il6* null mice, observing effects out to 4 weeks and 12 weeks. AAV-OSM caused muscle atrophy and fibrosis in the gastrocnemius, tibialis anterior, and quadriceps of the injected limb, but these effects were not observed on the non-injected side. In contrast, OSM induced both local and distant trabecular bone loss as shown by reduced bone volume, trabecular number, and thickness, and increased trabecular separation. OSM caused cardiac dysfunction including reduced ejection fraction and reduced fractional shortening.

*To whom correspondence should be addressed: Teresa A. Zimmers, PhD, 980 W. Walnut Street, Walther Hall, R3-C518, Indianapolis, IN 46202, Phone: 317-278-7289, zimmerst@iu.edu.

Author contributions: DJ, MW, AN, JR, AY, XZ, and DH carried out experiments and data collection. DJ, MW, AR, and TZ conducted data analysis. DJ, AR, LK, and TZ designed the studies. DJ and TZ wrote the manuscript. All authors have read and approved of the manuscript.

Limitations: Musculoskeletal disorders and cachexia affect both men and women [54]. This study included only male mice, limiting the understanding of the musculoskeletal effects of OSM to males. Further investigation is required to determine the effects of OSM in the muscle and bone of female mice and to understand the implications of this work for humans.

RNA-sequencing of cardiac muscle revealed upregulation of genes related to inflammation and fibrosis. None of these effects were different in IL-6 knockout mice. Thus, OSM induces local muscle atrophy, systemic bone loss, tissue fibrosis, and cardiac dysfunction independently of IL-6, suggesting a role for OSM in musculoskeletal conditions with these characteristics, including cancer cachexia.

Keywords

Oncostatin M; Interleukin-6; Skeletal Muscle; Bone; AAV; Atrophy; Fibrosis; Inflammation; IL6ST/GP130; Cachexia; Cardiac Dysfunction

INTRODUCTION

Musculoskeletal (MSK) diseases and disorders impair muscle, bone, joint, and overall physical health and result in a great burden on the United States healthcare system costing over 500 billion dollars each year [1]. The prevalence of MSK disorders increases with age, along with the risk of co-morbidities such as obesity and cancer; thus, there is a need for more therapeutic approaches and advances to treat musculoskeletal disorders [1, 2].

Cachexia manifests as severe musculoskeletal abnormalities. Cachexia is the progressive wasting of muscle, adipose tissue, and sometimes bone due to systemic inflammation and dysmetabolism [3, 4]. Cachexia is a feature of many acute and chronic disease conditions, including trauma and burns, as well as cancer, rheumatoid arthritis, organ failure, and HIV/AIDS [5]. In all these disorders, the presence of a wound, tumor, or a non-healing organ elicits local and distant production of cytokines and other mediators that together evoke the hallmarks of systemic wasting—lipolysis, skeletal and cardiac muscle catabolism, and as is increasingly recognized, bone loss [5–10]. In general, cachexia is associated with elevated levels of inflammatory cytokines including IL-1, IL-6, TNF-alpha, and Activin with evidence for activation of signaling pathways such as Janus Kinase/Signal Transducer and Activator of Transcription (JAK/STAT), Smad2/3/4, and phosphoinositide 3-kinase (PI3K) [7, 11, 12]. The IL-6 family consists of Interleukin-6 (IL-6), Oncostatin M (OSM), Leukemia Inhibitory Factor (LIF), Cardiotrophin-1 (CT-1), Ciliary Neurotrophic Factor (CNTF), Cardiotrophin-like Cytokine (CLC), and Interleukin-27 (IL-27) [13]. In the field of cachexia research, IL-6 is well-studied and there is emerging evidence for the role of LIF, CNTF, and CT-1 in muscle, cardiac, and bone wasting [14–16]. Other members of the IL-6 family of cytokines have been less characterized in cachexia, including Oncostatin M.

Oncostatin M (OSM) was first characterized to inhibit tumor cell proliferation but is now known to have roles in inflammatory disorders and fibrosis via effects on cell proliferation and differentiation and cytokine secretion. In mice, OSM binds to GP130 and recruits OSM receptor (OSMR) as a coreceptor; in humans, OSM-bound GP130 recruits either LIF receptor (LIFR) (type II receptor complex) or OSMR (type I receptor complex) as co-receptors to mediate signal transduction. Little is known of OSM in the pathogenesis of cachexia per se, although various activities of OSM suggest its potential to modulate systemic wasting. In adipose tissues, OSM inhibits adipocyte differentiation in vitro and can be secreted from adipose tissue macrophages [17]. In skeletal muscle, OSM inhibits

muscle stem cell differentiation and is secreted from muscle [18, 19]. In bone, OSM induces expression of RANKL, osteoclast formation, and functions in hematopoiesis and thrombocytosis. OSM functions to support bone formation and resorption [20, 21]. In the heart, OSM signaling is protective in cardiac regeneration [22], but OSM also promotes differentiation of cardiomyocytes and exacerbates cardiac failure [23]. To date, the effects of OSM manipulation on cardiac and skeletal muscle and bone have not been evaluated concurrently, demonstrating a need investigate the systemic effects of OSM in muscle and bone health.

Given the paucity of literature on OSM in systemic musculoskeletal disorders, this study aimed to examine the role of elevated OSM on muscle and bone. We used adeno-associated virus (AAV) to deliver OSM at high levels locally in muscle and lower levels systemically. Given that OSM is known to elicit expression of IL-6, we also sought to determine whether IL-6 was required for any OSM activities we identified via use of *Il6* null mice. Here we show that OSM induced hematological markers of inflammation, local skeletal muscle wasting and fibrosis, profound systemic bone loss, and cardiac dysfunction. All the effects observed were independent of the presence of IL-6. Thus, OSM can induce hallmark characteristics of cachexia—inflammation and tissue wasting. Overall, these studies support the need for investigation of OSM in specific systemic wasting conditions.

MATERIALS AND METHODS

OSM and OSMR expression data

To identify potential targets for cachexia, we used in silico analysis to determine expression of OSM and OSMR as recommended by [24]. Expression of OSM and OSMR in murine muscles was queried using MuscleDB by Laura D. Hughes, Karyn Esser, and Michael E. Hughes at muscledb.org [25]. Expression in human tissues was queried in Human Protein Atlas proteinatlas.org at https://www.proteinatlas.org/ENSG00000099985-OSM/tissue and https://www.proteinatlas.org/ENSG00000145623-OSMR/tissue [26].

Ethics

All experiments were conducted under protocol #11377 approved by the Institutional Animal Care and Use Committee at Indiana University School of Medicine (IUSM) and the Roudebush Veterans Administration Medical Center.

AAV

Adeno-associated viruses (AAVs) were serotype Capsid AAV-1 and ITR AAV-2, with the CAG promoter driving expression of murine OSM, AAV1-CAG-mOSM-WPRE (AAV-Osm), or no-insert AAV1-CAG-Null (AAV-Null) (Vector Biolabs, Malvern, PA, USA).

Animals

OSM levels reported in Figure 1 are from KrasG12D;Trp53R172H:Pdx1-cre (KPC) mice with autochthonic pancreatic cancer as reported in Zhong et al, 2022 [27].

For studies in Figures 2–12, *Il6*$^{-/-}$ B6.129S2-*Il6*^{tm1Kopf}/J (002650) and wildtype C57BL/6J (000664) (Jackson Laboratories, Bar Harbor, ME, USA) male mice were acclimated to the Laboratory Animal Resource Center at IUSM for 3-weeks prior to conducting the study. Mice were housed in a temperature-controlled room with a 12-hour light/dark cycle and maintained a standard rodent diet with ad libitum access to food and water. AAVs were diluted in sterile PBS (final volume 100 ul) and injected using a 29-1/2-gauge insulin syringe into the right gastrocnemius of 10-week-old mice under 2% isoflurane general anesthesia supplemented with O_2. The study involves three experiments: high titer at 4-days, and low titer at 4-weeks and 12-weeks. High titer: 10 wildtype mice were injected with $3x10^{11}$ genome copies/mL (gc/mL) AAV-Null, and 10 wildtype mice were injected with 8 x 10^{12} gc/mL AAV-Osm. Within 4 days following injection, 6 out of the 10 AAV-Osm mice were found dead and the study was terminated. Thus, 4 mice per group were included in the final analysis. The study was later repeated with 10 per group using 8 x 10^{12} gc/mL of either AAV-Null or AAV-Osm to collect blood at 4-days for OSM and IL-6 levels. Low titer: 4-week—5 mice of each genotype, wildtype and *Il6*$^{-/-}$, were injected with $2.6x10^{11}$ gc/mL AAV-Osm and 5 mice of each genotype, wildtype and *Il6*$^{-/-}$, were injected with $2.6x10^{11}$ gc/mL AAV-Null. 12-week—10 mice of each genotype, wildtype and *Il6*$^{-/-}$, were injected with $2.6x10^{11}$ gc/mL AAV-Osm and 10 mice of each genotype, wildtype and *Il6*$^{-/-}$, were injected with $2.6x10^{11}$ gc/mL AAV-Null. At week four of this 12-week study, 5 of the *Il6*$^{-/-}$ AAV-Osm mice were euthanized due to severe skin lesions and hair loss. The remaining 5 mice were treated with antibiotics until the lesions healed and were included in the final analysis. Thus, in all, 40 mice were injected but 35 mice were included in the final analysis.

Echocardiography

Echocardiography was performed to determine cardiac influence of WT and *Il6*$^{-/-}$ mice subjected to injection of either AAV-Null or AAV-Osm, at weeks 2, 4, and 10 after AAV injection using the Vevo® 2100 system (Fujifilm VisualSonics Inc., Toronto, Canada). Cardiac function and muscle mass were assessed on isoflurane anesthetized mice with a heart rate of 400-500 beats per minute. M-mode scanning of the left ventricular chamber was used for measurement of left ventricular mass (LV), ejection fraction (EF), fractional shortening (FS), LV internal diameter (diastole/systole) (LVIDd/s) and posterior wall thickness (diastole/systole) (PWTd/s).

Euthanasia and organ collection

Mice were euthanized under isoflurane general anesthesia via terminal cardiac puncture to collect blood followed by cervical dislocation. Muscle and organs were excised and weighed. Skeletal muscle was either snap frozen in liquid nitrogen or mounted on cork discs and frozen for 45 seconds in liquid nitrogen-cooled isopentane (2-methylbutane) (03551-4, Fisher Chemical, Waltham, MA USA) and stored in −80°C. Tissues were either snap frozen and stored in −80°C or fixed in neutral buffered formalin and stored in 70% ethanol in 4°C.

CBC and ELISA

Blood was collected and complete blood cell counts determined using the Heska Element HT5 (Loveland, CO USA). Mouse Oncostatin M Quantikine ELISA kit (MSM00) and Mouse Interleukin-6 Quantikine ELISA kit (M6000B) were used according the

manufacturer's instructions to measure cytokine levels in platelet-poor plasma from blood collected in EDTA microtainers.

RNA extraction and quantitative polymerase chain reaction

Total RNA was extracted from 30mg of quadriceps and the apex of the heart using a RNeasy Mini kit (Qiagen, 74104, Germantown, MD). Quality of RNA was measured using Agilent Bioanalyzer Nano RNA chip. Complementary DNA (cDNA) was synthesized using the Fisher Scientific Verso cDNA Synthesis Kit (AB1453B). Quantitative polymerase chain reaction was performed using TaqMan assay probes from Thermo Fisher Scientific found in Table 1: *Osm* Mm01193966_m1, *Osmr* Mm01307326_m1, *Bnip3* Mm01275600_g1, *Bnip3-L* Mm00786306_s1, *Trim63* Mm01185221_m1, *Fbxo32* Mm00499523_m1, *Tbp* Mm00446974_m1, *Postn* Mm01284919_m1, *Vim* Mm01333430_m1, and *Acta2* Mm00725412_s1.

RNA sequencing

RNA was evaluated for quantity and quality using Agilent Bioanalyzer 2100 Nano RNA chip. RNA was DNase treated using ThermoFisher Turbo DNA-Free kit (AM1907). For RNA quality, a RIN of 9 or higher was desired and used for processing; 100ng of total RNA was used for each sample. cDNA library preparation included mRNA purification/enrichment, RNA fragmentation, cDNA synthesis, ligation of index adaptors, and application following KAPA mRNA Hyperprep Kit prep (KK8581). Each resulting indexed library was quantified and its quality accessed by NovaSeq 6000; 5μL of 2nM pooled libraries per lane were denatured, neutralized, and applied to the cBot for flow cell deposition and cluster amplification before loading to 100bp paired-end sequencing (Illumina, Inc). Approximately 30-50 million reads per library were generated. A Phred quality score (Q score) was used to measure the quality of sequencing. More than 90% of the sequencing reads reached Q30 (99.9% base call accuracy). The sequence reads were mapped to the UCSC mm10 reference genome using STAR (Spliced Transcripts Alignment to a Reference) [28]. To evaluate the quality of the RNA-seq data, number of reads that fall into different annotated regions (exonic, intronic, splicing junction, intergenic, promoter, UTR, etc.) of the reference genes was determined with bamUtils 0.5.9 [29]. Low quality mapped reads (including reads mapped to multiple positions) were excluded and featureCounts 1.5.1 [30] was used to quantify the gene level expression. Differential gene expression analysis was performed with edgeR 3.28.1 [31]. Differentially expressed genes (fold change 1.5 $p<0.05$) between AAV-Osm and AAV-Null were visualized analyzed using Ingenuity Pathway Analysis (Qiagen). Pathways and ontology terms with $p<0.05$ were only considered for representation. The data discussed in this publication have been deposited in NCBI's Gene Expression Omnibus and are accessible through GEO series accession number GSE185996.

MicroCT for bone morphometry

Micro-computed tomography analysis was performed on dissected left and right femurs using a high-resolution desktop μCT (μCT-35; Scano Medical AG, Basel, Switzerland). The samples were scanned at 10μm resolution, 55kVp intensity with 0.5mm aluminum filter, and 400ms integration time. Femur lengths were measured prior to scanning and used to identify

a consistent reconstruction region. The distal femur metaphysis was analyzed and measured for medullary total volume (TV), trabecular bone volume (BV), trabecular thickness (Tb. Th), trabecular number (Tb. N), trabecular separation (Tb. Sp), and structural model index (SMI). At the midshaft region, cortical bone volume (Ct.BV) and cortical thickness (Ct. Th) were measured using standard procedures [32].

Tissue histology and immunohistochemistry

Frozen gastrocnemius and tibialis muscles were sectioned down to the midbelly using a Cryostat (Leica USA). 10mm sections were mounted on Superfrost Plus slides at −20°C. Hematoxylin & Eosin: H&E staining of gastrocnemius muscle was conducted as described [24]. Trichrome (Connective Tissue Stain): Sections of right gastrocnemius were stained using abcam150686 Trichrome Stain. Images were collected with the Zeiss Axio Microscope.

Statistical analysis

Data are reported at mean ± SD. P-values are reported. Unpaired t-test was performed for two group comparisons in Figure 2; otherwise, two-way ANOVA with Tukey's Multiple Comparisons post-test was performed to assess significance between genotypes (WT and *Il6*) and treatment (AAV-Null or AAV-Osm) using GraphPad Prism version 8.3.1 for Mac, GraphPad Software, La Jolla California USA, www.graphpad.com.

RESULTS

Plasma OSM is elevated in pancreatic cancer cachexia

Seeking potential mediators of cachexia in pancreatic cancer, we tested plasma levels of the GP130 family cytokine, OSM, in a genetically engineered mouse model (GEMM) of pancreatic cancer (KPC mice). Plasma levels were increased from 0 pg/mL to 377 pg/mL (AVG: 49.1 ± SD: 93.6) (Figure 1A), suggesting that OSM might contribute to the known systemic effects of pancreatic cancer, including adipose, skeletal muscle, and cardiac wasting and dysfunction.

OSM/OSMR expression

MuscleDB RNAseq data of murine smooth, cardiac, and skeletal muscle shows that OSM is minimally detected, while OSMR transcripts are expressed across all these muscle types, including limb muscles (Figure 1B), but with greater expression in cardiac versus skeletal muscle. Per the Human Protein Atlas consensus dataset, in humans, OSM expression is largely restricted to bone marrow (Figure 1C) and granulocytes and monocytes (not shown), while OSMR expression is widely expressed across tissue types (Figure 1D). Antibody staining of human muscle in the Human Protein Atlas shows high expression of OSMR but not OSM in myofibers (not shown). These data suggest that circulating and local blood cell derived OSM might signal though OSMR in cardiac and skeletal muscle in normal and pathological conditions.

High dose AAV-Osm caused hepatomegaly, adipose loss, inflammation, but not muscle loss

To determine the effects of elevating OSM systemically, we over-expressed OSM via AAV-Osm injected into the gastrocnemius, expecting that viral production of OSM would elevate signaling both locally and globally. Injection of high titer AAV-Osm resulted in sudden death of 6 of 10 injected mice within 4 days, provoking euthanasia of the remaining mice (Figure 2A–B). This sudden death was not due to viral titer, as simultaneous studies with 8 mice per group injected with matched titers of viruses engineered to over-express leukemia inhibitor factor (LIF), cardiotrophin-1 (CTF-1), and ciliary neurotrophic factor (CNTF) did not show any mortality (data not shown). Thus, mortality was specific to AAV-Osm.

AAV-Osm elevated circulating levels of OSM to 1074 - 62702 pg/mL (AVG: 12010 ± SD: 20316) ($p<0.0001$) and IL-6 to 31 - 1,571 pg/mL (AVG: 322.1 ± SD: 479.8) ($p=0.0002$) in plasma compared to AAV-Null (Figure 2C). AAV-Osm mice presented with hepatomegaly (*p<0.001*) and fat loss (*p=0.0446*) but no differences in the heart or spleen mass (Figure 2D). High titer AAV-Osm did not demonstrate an effect on ipsilateral (injected) or contralateral (non-injected) limb skeletal muscles—gastrocnemius, quadriceps, tibialis anterior (Figure 2E). AAV-Osm decreased mean corpuscular hemoglobin concentration (*p=0.0090*), increased platelet count (*p=0.0169*), increased neutrophil count (*p=0.0014*), increased neutrophil-to-lymphocyte ratio (*p=0.0006*) but did not change overall white blood cell count (Figure 2F). In the subsequent studies, to avoid sudden death, achieve physiological levels of OSM, and evaluate a musculoskeletal effect in mice, we reduced the viral titer to 10^{11} and to assess whether OSM effects required IL-6 production, we included a cohort of *Il6*$^{-/-}$ mice.

Low dose AAV-Osm causes local muscle and fat loss, hepato-splenomegaly at 4 weeks

In the low dose study, 10 wildtype mice and 10 *Il6*$^{-/-}$ mice were separated into four experimental groups. Wildtype mice were injected with AAV-Osm (n=5) and AAV-Null (n=5), and *Il6*$^{-/-}$ mice were injected with AAV-Osm (n=5) and AAV-Null (n=5) via an intramuscular injection in the right gastrocnemius. The study was conducted for 4 weeks (Figure 3A).

From blood draws during week 1 of this study, we determined OSM circulated at 76.9 pg/mL (n=1) in a WT AAV-Osm mouse compared to WT AAV-Null 19.63 pg/mL - 21.45 pg/mL (AVG: 20.8 ± SD: 1.1) (n=3). In *Il6*$^{-/-}$ AAV-Osm mice, OSM was increased to 66 pg/mL - 101.4 pg/mL (AVG: 80.2 ± SD: 18.7) (n=3) compared to *Il6*$^{-/-}$ AAV-Null mice 18.7 pg/mL - 24.1 pg/mL (AVG: 21.4 ± SD: 2.7) (n=3). At euthanasia at week 4, a terminal cardiac blood draw showed that in WT mice AAV-Osm elevated circulating OSM (53-120 pg/mL) (AVG: 84.0 ± SD: 25.3) but not IL-6 (0 pg/mL) (AVG: 0 ± SD: 0) (Figure 3B–C). AAV-Osm mice presented with cardiac hypertrophy (*p=0.0009*), hepatomegaly (*p=0.0003*), splenomegaly (*p<0.0001*) and fat loss (*p=0.0193*) (Figure 3D). AAV-Osm mice had induction of local muscle loss—gastrocnemius (GSN) (*p=0.0394*) in wildtype mice (Figure 3E). Muscle loss was not observed the contralateral side, or in mice with AAV-Null. AAV-Osm in *Il6*$^{-/-}$ mice elevated circulating OSM (100-160 pg/mL) (AVG: 127.5 ± 25.1) but, as expected, not IL-6 (0 pg/mL) (AVG: 0 ± SD: 0) (Figure 3F–G).

AAV-Osm *Il6*$^{-/-}$ mice presented with hepatomegaly (*p<0.0001)*, splenomegaly (*p<0.0001*) and fat loss (*p=0.0124*), but with no differences in cardiac mass (Figure 3H). AAV-Osm *Il6*$^{-/-}$ mice had muscle loss of the gastrocnemius (GSN) (p=0.0015), tibialis anterior (TA) (*p=0.0164*) and quadriceps (QUAD) (*p=0.0002*) on the injected side (Figure 3I); however, muscle loss was not observed the contralateral side, or in mice with AAV-Null.

Low dose AAV-Osm causes local muscle loss and fibrosis

In the low titer study, 20 wildtype mice and 20 *Il6*$^{-/-}$ mice were separated into four experimental groups. Wildtype mice were injected with AAV-Osm (n=10) and AAV-Null (n=10), and *Il6*$^{-/-}$ mice were injected with AAV-Osm (n=10) and AAV-Null (n=10) via an intramuscular injection in the right gastrocnemius. The study was conducted for 12 weeks (Figure 4A).

At euthanasia, AAV-Osm induced hepatomegaly (*p=0.0118)*, and fat loss (*p=0.0039*) but no cardiac mass differences or splenomegaly in wildtype mice (Figure 4B). AAV-Osm mice had induced local skeletal muscle loss in the ipsilateral gastrocnemius (GSN) (*p<0.0001)*, in the ipsilateral quadriceps (QUAD) of WT AAV-Osm (*p=0.0002*), and in the ipsilateral tibialis anterior (TA) of WT AAV-Osm (*p=0.0031)*. There was no muscle loss observed in mice injected with AAV-Null. As well, there was no muscle atrophy observed in the contralateral, uninjected skeletal muscles of either AAV-Osm or AAV-Null mice (Figure 4C). AAV-Osm induced hepatomegaly (*p=0.0212)*, and fat loss (*p=0.0005*) but no cardiac mass differences or splenomegaly in wildtype mice (Figure 3D). AAV-Osm mice had induced local skeletal muscle loss in the ipsilateral gastrocnemius (GSN) (*p<0.0001)*, in the ipsilateral quadriceps (QUAD) (*p<0.0001*), and in the ipsilateral tibialis anterior (TA) (*p=0.0030).* There was no muscle loss observed in mice injected with AAV-Null. As well, there was no muscle atrophy observed in the contralateral, uninjected skeletal muscles of either AAV-Osm or AAV-Null mice (Figure 4E). AAV-Osm caused muscle degeneration and fibrosis on the ipsilateral side in both WT and *Il6*$^{-/-}$ mice, as shown by H&E and trichrome stain of the right gastrocnemius. This effect was not observed on the contralateral side nor on either side in mice injected with AAV-Null (Figure 4F). Because we did not observe skeletal muscle atrophy in the contralateral limb of AAV-Osm mice, we conducted the remainder of the muscle analysis on the ipsilateral limb.

To determine changes in gene expression of atrophy markers, we carried out qPCR for *Osm* and *Osmr*, as well as pro-atrophy genes including the skeletal muscle-specific ubiquitin ligases, *Trim63* and *Fbxo32*, as well as the autophagy markers, *Bnip3L* and *Bnip3* in the right quadriceps (Figure 5). The expression of *Osmr* was elevated in WT AAV-Osm compared to WT AAV-Null (p=0.0076) and *Il6*$^{-/-}$ AAV-Osm compared to *Il6*$^{-/-}$ AAV-Null (*p=0.0003*), although the expression of *Osm* was not consistently changed in wildtype or *Il6*$^{-/-}$ mice in any condition in the quadriceps (Figure 5A). In the injected gastrocnemius of wildtype and *Il6*$^{-/-}$ mice, qPCR shows there was a trend in *Osm* expression in WT AAV-Osm 47.6-fold-467.5-fold (AVG: 291.3 ± SD: 218.0) (n=3) compared to WT AAV-Null 0.68-fold-1.5-fold (AVG: 1.05 ± SD: 0.43) (n=3) and trended increase in *Il6*$^{-/-}$ AAV-Osm was 401.3-fold and 628.4-fold (n=2) compared to *Il6*$^{-/-}$ AAV-Null was 0.70-fold-1.3-fold (AVG: 0.98 ± SD: 0.35) (n=3) (Figure 5A). In contrast to results at 4 weeks, by 12 weeks

circulating Osm level was not elevated in AAV-Osm mice (WT: 5pg/mL and *Il6*$^{-/-}$: 4.5 pg/mL, n=3 pooled) versus AAV-Null. Despite the wasted phenotype, *Fbxo32* expression was decreased in *Il6*$^{-/-}$ AAV-Osm compared to *Il6*$^{-/-}$ AAV-Null (*p=0.0242*), and *Trim63*, *Bnip3L*, and *Bnip3* gene expression were not changed with AAV-Osm (Figure 5B). These histological and gene expression results indicate that by the time of our analysis, the injected muscle tissue was largely replaced by fibrotic tissue, with elimination of cells that once expressed the recombinant OSM and muscle-specific markers.

AAV-Osm lowers trabecular bone at 12 weeks

Bone loss is observed in mouse models of colorectal cachexia [33], so we sought to quantify changes in bone with AAV-Osm (Figure 6). We conducted MicroCT (μCT) analysis on the ipsilateral and contralateral femur from wildtype and *Il6*$^{-/-}$ mice to measure medullary total volume (TV), trabecular bone volume (BV), trabecular thickness (Tb. Th), trabecular number (Tb. N), trabecular separation (Tb. Sp) and structural model index (SMI) and at the midshaft region, to measure cortical bone volume (Ct. BV) and cortical thickness (Ct. Th).

In wildtype mice, AAV-Osm treatment induced a significant decrease in BV/TV of ipsilateral (*p<0.0001*) and contralateral (*p=0.0011*) femur, in Tb.Th of ipsilateral (*p=0.0040*) but not contralateral femur, in Tb.Sp of ipsilateral (*p<0.0001*) and contralateral (*p=0.0006*) femur, in Tb.N of ipsilateral (*p<0.0001*) and contralateral (*p=0.0003*) femur, Ct.Th of ipsilateral (*p=0.0001*) and contralateral (*p=0.0031*) femur, and Ct. BV of contralateral (*p=0.0270*) but not ipsilateral femur. In *Il6*$^{-/-}$ mice, AAV-Osm treatment induced a significant decrease in BV/TV of ipsilateral (*p<0.0001*) and contralateral (*p<0.0001*) femur, in Tb.Th of ipsilateral (*p=0.0036*) and contralateral (p=0.0368) femur, in Tb.Sp of ipsilateral (*p=0.0011*) and contralateral (*p=0.124*) femur, in Tb.N of ipsilateral (*p<0.0020*) and contralateral (*p=0.0134*) femur, Ct.Th of contralateral (*p=0.0036*) but not ipsilateral femur, and Ct. BV of contralateral (*p=0.0172*) but not ipsilateral femur (Figure 6A). Representative cross-sectional images of the ipsilateral distal femur demonstrate trabecular loss in the wildtype and *Il6*$^{-/-}$ AAV-Osm mice and altered cortical bone surface with AAV-Osm (Figure 6B).

AAV-Osm induces cardiac dysfunction

Cardiac dysfunction occurs in cancer cachexia. To evaluate effects of AAV-Osm on cardiac function over the course of the study, we monitored cardiac function longitudinally by echocardiography. In week 2, there was no difference in ejection fraction (EF%), fractional shortening (FS%), and LV Mass-c (mg) with AAV-Osm (Figure 7A). By week 4, there was significantly reduced EF% observed (WT: *p=0.0035*; *Il6*$^{-/-}$: *p=0.0018*) AAV-Osm mice and FS% *p=0.0003* in *Il6*$^{-/-}$ in AAV-Osm mice. Reduction of EF% was sustained at week 10, with AAV-Osm WT: *p=0.0120*; *Il6*$^{-/-}$: *p=0.0026*); and there was reduction of FS% with AAV-Osm (WT: *p=0.0111*; *Il6*$^{-/-}$: *p=0.0022*). There was no difference in LV mass with AAV-Osm over time (Figure 7B, 7C).

AAV-Osm has minimal effect on cardiac size at 12 weeks

Over the course of 10 weeks, there was no difference in left ventricular internal diameter (diastole/systole) (LVIDd/s) or posterior wall thickness (diastole/systole) (PWTd/s) with

AAV-Osm in wildtype mice (Figure 8A). In week 4, there was an increase in LVIDd with *Il6*$^{-/-}$ AAV-Osm (*p=0.0487*) but no difference in LVIDs, PWTd/s in *Il6*$^{-/-}$ mice (Figure 8B). Representative H&E and trichrome images of the hearts from AAV-Null and AAV-Osm mice demonstrate no significant differences in cardiac morphology (Figure 8C).

AAV-Osm induces cardiac inflammation at 12 weeks

To determine the gene expression changes coincident with cardiac dysfunction induced by AAV-Osm, RNA-sequencing was performed on wildtype AAV-Null and AAV-Osm hearts. Gene signatures of inflammation, cardiac dysfunction, and fibrosis were observed with AAV-Osm. Upregulation of Osmr and chemokine and chemokine receptor genes Csf2rb, Csf2rb2, and Ccl9 and downregulation of genes Dpp4, Ccl12, Ccl2, Cxcl9, and Cxcr2 suggested a late immune response to cardiac disease with AAV-Osm (Figure 9A). There was elevated expression of proliferation markers such as Scgb3a1, and metabolic and oxidative stress related genes such as Lepr, Angptl4, Oser1, Casp4, and clock and circadian genes such as Ciart, Per3, Per1 (Figure 9B). There was an increase in platelet activation genes and cell adhesion/activation genes such as Selp, Lgals4, Esm1, Pcdhgb, Pcdhga, and downregulation of metalloproteinases and collagen genes such as Timp4, Mmp, Nes, Col13a1, Col4a6, and Col4a3 (Figure 9C). The top 10 canonical pathways activated by AAV-Osm were Oncostatin M Signaling, Glucocorticoid Receptor Signaling, Hepatic fibrosis/hepatic stellate cell activation, Granulocyte Adhesion and Diapedesis, Agranulocyte Adhesion and Diapedesis, Ferroptosis Signaling Pathway, Atherosclerosis Signaling, Acute Phase Response Signaling, Epithelial Adherens Junction signaling, and LXR/RXR activation (Figure 10). To determine changes in gene expression with cardiac fibrosis in the *Il6* null mice, qPCR was conducted for *Osm*, *Osmr*, *Acta*, *Vim*, and *Postn* in the *Il6*$^{-/-}$ AAV-Osm and AAV-Null hearts. *Osmr* was elevated in *Il6*$^{-/-}$ AAV-Osm (*p=0.0470*) but Osm, Acta, Vim, and Postn were not changed (Figure 11).

DISCUSSION

Musculoskeletal disorders impair overall physical health yet there are limited therapeutic approaches to treat advanced disease. Cachexia, a musculoskeletal disorder, presents as loss of overall body weight and muscle weight, and sometimes bone atrophy due to inflammation and dysmetabolism. The inflammatory cytokines IL-6 and LIF are well-studied in the progression of cachexia but there is minimal evidence for roles of the other IL-6 family members such as OSM. This study aimed to determine the effects of OSM in mediating muscle loss in mice without cancer or other underlying diseases and differentiate these activities from those of IL-6.

In our study, a high dose of OSM increased platelet count in mice and activated thrombocytopoiesis as shown by complete blood count and elevated OSM and IL-6 plasma levels driving a systemic inflammatory response. The high dose resulted in the sudden lethality and moribund state of some animals. Our observation is similar to the Wallace et al, Juan et al, Kerr et al studies, respectively where injecting recombinant human or bovine OSM in mice induced lethality, hematopoietic effects, and an intramuscular injection of an adenovirus expressing murine OSM elevated IL-6 plasma expression, respectively

[34–37]. Thus our observations of systemic inflammatory and thrombocytopoetic effects were consistent with described activities of OSM, mediated through IL-6. Thus, to better understand the in vivo effects of OSM absent from IL-6, we repeated the in vivo experiments in *Il6* null mice. Moreover, given that the systemic effect of the high titer limited the study to four days and did not produce muscle loss, or physiological levels of OSM, we lowered the dose and repeated the study and focused on monitoring body composition and cardiac function— effects altered in cachexia.

We demonstrate that increasing circulating OSM to levels similar to those in cancer cachexia induced musculoskeletal wasting effects and that none of these effects were IL-6 dependent. Previous studies have demonstrated a role for OSM in regulating muscle size and regeneration in vitro [18, 38]. Along with evidence for OSM and IL-6 as myokines and elevated OSM expression in muscle during exercise induced inflammation [39, 40]. Additionally, recombinant OSM can mediate myotube atrophy in vitro [19]. In our study, we were unable to identify changes in gene expression of atrophy markers, but *Osmr* was elevated in muscle of wildtype and IL-6 mice. The extent of skeletal muscle loss, the muscle being nearly obliterated, and the remaining tissue fibrotic in nature with OSM—all minimized the potential to determine gene expression level changes. Notwithstanding, our study extends the in vitro studies previously observed and demonstrates an induction of muscle loss by OSM in vivo, although only locally near the site of production. Systemic loss of muscle was not observed, nor was there wasting of cardiac muscle. In normal tissue, *Osmr* expression is greater in cardiac than skeletal muscle. Over the course of 4 weeks we observed local muscle loss, so we observe both cardiac dysfunction and skeletal muscle loss by chronic exposure. However, the mechanisms for OSM mediating muscle atrophy in vivo and in cachexia are still unclear.

OSM is expressed in blood cells and promotes hematopoiesis, marrow fibrosis, and bone cell differentiation and formation [34–37]. IL-6 binding to IL-6 receptor stimulates osteoclast formation and mediates osteoclastogenesis by promoting RANKL release [41, 42]. However, lack of *Il6* expression is not associated with a defect in osteoclast formation or trabecular bone mass [20, 42]. In our findings, OSM lowered trabecular bone. Walker et al. treated *Osmr* null mice with recombinant OSM and showed that OSM promoted bone formation via leukemia inhibitory factor receptor signaling [43]. However, our findings suggest Osm/Osmr signaling mediate bone loss after chronic exposure. In prior work using a model overexpressing OSM in a mouse knee joint, local OSM induced cartilage inflammation, fibrosis, and destruction and bone formation. Moreover, OSM has been reported to regulate bone cell differentiation and proliferation; however, contrasting evidence suggest high expression of OSM can induce bone catabolism although the effects of overexpression are site specific [44–47]. Our findings are similar to the OSM-induced bone destruction described in previous publications additionally we did not observe differences in osteoclast number.

OSM induced cardiac dysfunction over time. Exposure of OSM over 4 weeks mediated cardiac hypertrophy in wildtype mice, although cardiac mass was unchanged at the end of 12 weeks between all comparisons and groups. Given the effects on cardiac dysfunction, we performed RNA-sequencing in the wildtype mice with OSM and we identified upregulated

genes involved in inflammation and fibrosis. Because there were no differences in cardiac dysfunction between *Il6*$^{-/-}$ and wildtype mice, we inferred the effects of OSM does not require IL-6 and we suspect there would be upregulation of genes related to inflammation and fibrosis in the *Il6*$^{-/-}$ AAV-Osm hearts. RNA-sequencing results from the cardiac muscle confirmed activation of inflammatory signaling pathways in mice overexpressed with OSM likely causing the cardiac dysfunction demonstrated by echocardiography. Previous published reports suggest IL-6 does not alter morpho-functional cardiac effects but mediates physiological and inflammatory markers during exercise [48]. Similarly, there are reported effects of OSM in cardiac failure and inflammation. OSM is elevated in patients with heart failure, mediates cardiac fibrosis, and is essential for cardiomyocyte proliferation and heart regeneration, and targeting OSMR protects against cardiac failure, however, the effects of OSM are disease specific and other literature suggests OSM promotes angiogenesis and preserves cardiac function [22, 23, 49–51]. In the heart, OSM has a pro-atherosclerotic function and can mediate cardiac repair but chronic exposure with OSM can result in cardiac dysfunction in some models [18, 52]. The cardiac effects from our study are in line the prior literature linking OSM to cardiac dysfunction.

Finally, the muscle and bone effects seen in our study were similar between wild-type and IL6 knockouts, demonstrating the functions of OSM in the musculoskeletal system is not dependent on IL-6.

The importance of muscle-bone crosstalk is essential in understanding systemic effects in musculoskeletal disease. The data here show local muscle loss and a systemic bone loss. We speculate the systemic bone effect was mediated in part by OSM-induced muscle loss and fibrosis resulting in an injured muscle that might lead to reduced activity and disuse atrophy. However, when animal activity was monitored, we did not observe differences in average speed, resting, rearing, or ambulatory movement with AAV-Osm (data not shown). Moreover, TRAP staining of a subset of femurs did not reveal a difference in osteoclast number (data not shown). Therefore, future studies would need to identify the molecular mechanisms that drive the muscle bone crosstalk and OSM/OSMR signaling.

Currently there is scant evidence to suggest OSM might mediate cachexia in cancer or other conditions. Barton et al, demonstrate that in a murine lung cancer model, OSM expression was detected in the spleen of wildtype mice [53]. Here we show that OSM was elevated in a mouse model of pancreatic cancer cachexia, and that similar levels of OSM led muscle and bone loss, adipose loss, hepatomegaly, cardiac dysfunction, and systemic inflammation in vivo suggesting importance for OSM in cancer cachexia and other musculoskeletal diseases (Figure 12). Our future studies will evaluate the effects of OSM in cancer cachexia by examining muscle, bone, heart function, and muscle morphometry in models of pancreatic and other cancers.

Acknowledgements:

DJ was supported by the Indiana University Simon Comprehensive Cancer Center Cancer Biology Training Program and the Indiana University Adam W. Herbert Graduate Fellowship. These studies were supported in part by grants from the National Institutes of Health 1F31CA265168 (DJ), R01CA122596 (TZ), R01CA194593 (TZ), and R01GM137656 (TZ, LK), R01AR053237 (AR), R56HL139967 (MW), T32HL007910 (JR), the Veterans Administration I01BX004177 and I01CX002046 (TZ), the IU Simon Comprehensive Cancer Center

(P30CA082709), and the Walther Cancer Foundation. The authors thank Tewfik Hamidi, Brittany Counts, Omnia Gaafer, and Emmarie Ballard for assistance on tissue collection. Sequencing was carried out by the Center for Medical Genomics and histology by the Histology Core, supported in part by NIH grants P30CA023168 and UL1TR002529. Illustrations were created using Servier Medical Art by Servier and licensed under a Creative Commons Attribution 3.0 Unported License.

Conflict of Interest:

TZ has received payment for consulting on cancer cachexia and is Scientific Advisory Board Member of Emmyon, Inc and PeleOS, LL. These arrangements have no bearing on the research reported here. The other authors have no conflicts of interest to declare.

REFERENCES

1. March L, et al. , Burden of disability due to musculoskeletal (MSK) disorders. Best Pract Res Clin Rheumatol, 2014. 28(3): p. 353–66. [PubMed: 25481420]
2. Tisdale MJ, Biology of cachexia. Journal of the National Cancer Institute, 1997. 89(23): p. 1763–73. [PubMed: 9392617]
3. Baracos VE, Mazurak VC, and Bhullar AS, Cancer cachexia is defined by an ongoing loss of skeletal muscle mass. Ann Palliat Med, 2019. 8(1): p. 3–12. [PubMed: 30685982]
4. Baracos VE, et al. , Cancer-associated cachexia. Nat Rev Dis Primers, 2018. 4: p. 17105. [PubMed: 29345251]
5. Cohen S, Nathan JA, and Goldberg AL, Muscle wasting in disease: molecular mechanisms and promising therapies. Nat Rev Drug Discov, 2015. 14(1): p. 58–74. [PubMed: 25549588]
6. Bonetto A, et al. , Differential Bone Loss in Mouse Models of Colon Cancer Cachexia. Front Physiol, 2016. 7: p. 679. [PubMed: 28123369]
7. Matthys P and Billiau A, Cytokines and cachexia. Nutrition, 1997. 13(9): p. 763–70. [PubMed: 9290087]
8. Graul AI, Stringer M, and Sorbera L, Cachexia. Drugs Today (Barc), 2016. 52(9): p. 519–529. [PubMed: 27883118]
9. Anker MS, et al. , Advanced cancer is also a heart failure syndrome - an hypothesis. Eur J Heart Fail, 2020.
10. Zimmers TA, Fishel ML, and Bonetto A, STAT3 in the systemic inflammation of cancer cachexia. Semin Cell Dev Biol, 2016. 54: p. 28–41. [PubMed: 26860754]
11. Fearon KC, Glass DJ, and Guttridge DC, Cancer cachexia: mediators, signaling, and metabolic pathways. Cell Metab, 2012. 16(2): p. 153–66. [PubMed: 22795476]
12. Egerman MA and Glass DJ, Signaling pathways controlling skeletal muscle mass. Crit Rev Biochem Mol Biol, 2014. 49(1): p. 59–68. [PubMed: 24237131]
13. Rose-John S, Interleukin-6 Family Cytokines. Cold Spring Harb Perspect Biol, 2018. 10(2).
14. Gao S, et al. , Acute myotube protein synthesis regulation by IL-6-related cytokines. American Journal of Physiology-Cell Physiology, 2017. 313(5): p. C487–C500. [PubMed: 28768641]
15. Rupert JE, et al. , IL-6 Trans-Signaling and Crosstalk Among Tumor, Muscle and Fat Mediate Pancreatic Cancer Cachexia. bioRxiv, 2020: p. 2020.09.16.300798.
16. Jengelley DHA and Zimmers TA, The Role of Interleukin-6/GP130 Cytokines in Cancer Cachexia, in Textbook of Systemic Effects of Advanced Cancer. 2022, Springer
17. Sanchez-Infantes D, et al. , Oncostatin m is produced in adipose tissue and is regulated in conditions of obesity and type 2 diabetes. J Clin Endocrinol Metab, 2014. 99(2): p. E217–25. [PubMed: 24297795]
18. Xiao F, et al. , Oncostatin M inhibits myoblast differentiation and regulates muscle regeneration. Cell Res, 2011. 21(2): p. 350–64. [PubMed: 20956996]
19. Miki Y, et al. , Oncostatin M induces C2C12 myotube atrophy by modulating muscle differentiation and degradation. Biochem Biophys Res Commun, 2019. 516(3): p. 951–956. [PubMed: 31272716]

20. Sims NA, Cell-specific paracrine actions of IL-6 family cytokines from bone, marrow and muscle that control bone formation and resorption. Int J Biochem Cell Biol, 2016. 79: p. 14–23. [PubMed: 27497989]
21. Pedersen BK and Febbraio MA, Muscle as an endocrine organ: focus on muscle-derived interleukin-6. Physiol Rev, 2008. 88(4): p. 1379–406. [PubMed: 18923185]
22. Kubin T, et al. , Oncostatin M is a major mediator of cardiomyocyte dedifferentiation and remodeling. Cell Stem Cell, 2011. 9(5): p. 420–32. [PubMed: 22056139]
23. Gruson D, et al. , Elevation of plasma oncostatin M in heart failure. Future Cardiol, 2017. 13(3): p. 219–227. [PubMed: 28585906]
24. Rupert JE, Jengelley DHA, and Zimmers TA, In Vitro, In Vivo, and In Silico Methods for Assessment of Muscle Size and Muscle Growth Regulation. Shock, 2020. 53(5): p. 605–615. [PubMed: 31939770]
25. Terry EE, et al. , Transcriptional profiling reveals extraordinary diversity among skeletal muscle tissues. Elife, 2018. 7.
26. Karlsson M, et al. , A single-cell type transcriptomics map of human tissues. Sci Adv, 2021. 7(31).
27. Zhong X, et al. , Sex specificity of pancreatic cancer cachexia phenotypes, mechanisms, and treatment in mice and humans: role of Activin. J Cachexia Sarcopenia Muscle, 2022.
28. Dobin A, et al. , STAR: ultrafast universal RNA-seq aligner. Bioinformatics, 2013. 29(1): p. 15–21. [PubMed: 23104886]
29. Breese MR and Liu Y, NGSUtils: a software suite for analyzing and manipulating next-generation sequencing datasets. Bioinformatics, 2013. 29(4): p. 494–6. [PubMed: 23314324]
30. Liao Y, Smyth GK, and Shi W, featureCounts: an efficient general purpose program for assigning sequence reads to genomic features. Bioinformatics, 2014. 30(7): p. 923–30. [PubMed: 24227677]
31. Robinson MD, McCarthy DJ, and Smyth GK, edgeR: a Bioconductor package for differential expression analysis of digital gene expression data. Bioinformatics, 2010. 26(1): p. 139–40. [PubMed: 19910308]
32. Robling AG, et al. , Sost, independent of the non-coding enhancer ECR5, is required for bone mechanoadaptation. Bone, 2016. 92: p. 180–188. [PubMed: 27601226]
33. Huot JR, et al. , MC38 Tumors Induce Musculoskeletal Defects in Colorectal Cancer. Int J Mol Sci, 2021. 22(3).
34. Wallace PM, et al. , Regulation of inflammatory responses by oncostatin M. J Immunol, 1999. 162(9): p. 5547–55. [PubMed: 10228036]
35. Juan TS, et al. , Mice overexpressing murine oncostatin M (OSM) exhibit changes in hematopoietic and other organs that are distinct from those of mice overexpressing human OSM or bovine OSM. Veterinary Pathology, 2009. 46(1): p. 124–37. [PubMed: 19112126]
36. Wallace PM, et al. , Thrombocytopoietic properties of oncostatin M. Blood, 1995. 86(4): p. 1310–5. [PubMed: 7632937]
37. Wallace PM, et al. , In vivo properties of oncostatin M. Ann N Y Acad Sci, 1995. 762: p. 42–54. [PubMed: 7545375]
38. Sampath SC, et al. , Induction of muscle stem cell quiescence by the secreted niche factor Oncostatin M. Nat Commun, 2018. 9(1): p. 1531. [PubMed: 29670077]
39. Hojman P, et al. , Exercise-induced muscle-derived cytokines inhibit mammary cancer cell growth. Am J Physiol Endocrinol Metab, 2011. 301(3): p. E504–10. [PubMed: 21653222]
40. Pedersen BK, Steensberg A, and Schjerling P, Muscle-derived interleukin-6: possible biological effects. J Physiol, 2001. 536(Pt 2): p. 329–37. [PubMed: 11600669]
41. Ishimi Y, et al. , IL-6 is produced by osteoblasts and induces bone resorption. J Immunol, 1990. 145(10): p. 3297–303. [PubMed: 2121824]
42. Harmer D, Falank C, and Reagan MR, Interleukin-6 Interweaves the Bone Marrow Microenvironment, Bone Loss, and Multiple Myeloma. Frontiers in Endocrinology, 2019. 9(788).
43. Walker EC, et al. , Oncostatin M promotes bone formation independently of resorption when signaling through leukemia inhibitory factor receptor in mice. J Clin Invest, 2010. 120(2): p. 582–92. [PubMed: 20051625]

44. Kerr C, et al. , Adenovirus vector expressing mouse oncostatin M induces acute-phase proteins and TIMP-1 expression in vivo in mice. Journal of interferon & cytokine research : the official journal of the International Society for Interferon and Cytokine Research, 1999. 19(10): p. 1195–1205. [PubMed: 10547160]
45. de Hooge AS, et al. , Adenoviral transfer of murine oncostatin M elicits periosteal bone apposition in knee joints of mice, despite synovial inflammation and up-regulated expression of interleukin-6 and receptor activator of nuclear factor-kappa B ligand. Am J Pathol, 2002. 160(5): p. 1733–43. [PubMed: 12000725]
46. Hui W, et al. , A model of inflammatory arthritis highlights a role for oncostatin M in pro-inflammatory cytokine-induced bone destruction via RANK/RANKL. Arthritis Res Ther, 2005. 7(1): p. R57–64. [PubMed: 15642143]
47. Sims NA, Influences of the IL-6 cytokine family on bone structure and function. Cytokine, 2021. 146: p. 155655. [PubMed: 34332274]
48. da Rocha AL, et al. , Interleukin-6 ablation does not alter morphofunctional heart characteristics but modulates physiological and inflammatory markers after strenuous exercise. Cytokine, 2021. 142: p. 155494. [PubMed: 33765652]
49. Abe H, et al. , Macrophage hypoxia signaling regulates cardiac fibrosis via Oncostatin M. Nature Communications, 2019. 10(1): p. 2824.
50. Li Y, et al. , gp130 Controls Cardiomyocyte Proliferation and Heart Regeneration. Circulation, 2020. 142(10): p. 967–982. [PubMed: 32600062]
51. Zhang X, et al. , OSM Enhances Angiogenesis and Improves Cardiac Function after Myocardial Infarction. BioMed Research International, 2015. 2015: p. 317905. [PubMed: 26146616]
52. Sims NA and Quinn JM, Osteoimmunology: oncostatin M as a pleiotropic regulator of bone formation and resorption in health and disease. Bonekey Rep, 2014. 3: p. 527. [PubMed: 24876928]
53. Barton BE and Murphy TF, Cancer cachexia is mediated in part by the induction of IL-6-like cytokines from the spleen. Cytokine, 2001. 16(6): p. 251–7. [PubMed: 11884029]
54. Zhong X and Zimmers TA, Sex Differences in Cancer Cachexia. Curr Osteoporos Rep, 2020.

HIGHLIGHTS

- Exogenous OSM mediates muscle wasting and bone wasting in vivo
- Exogenous OSM induces cardiac dysfunction and inflammation
- Effects of OSM are not dependent on IL-6

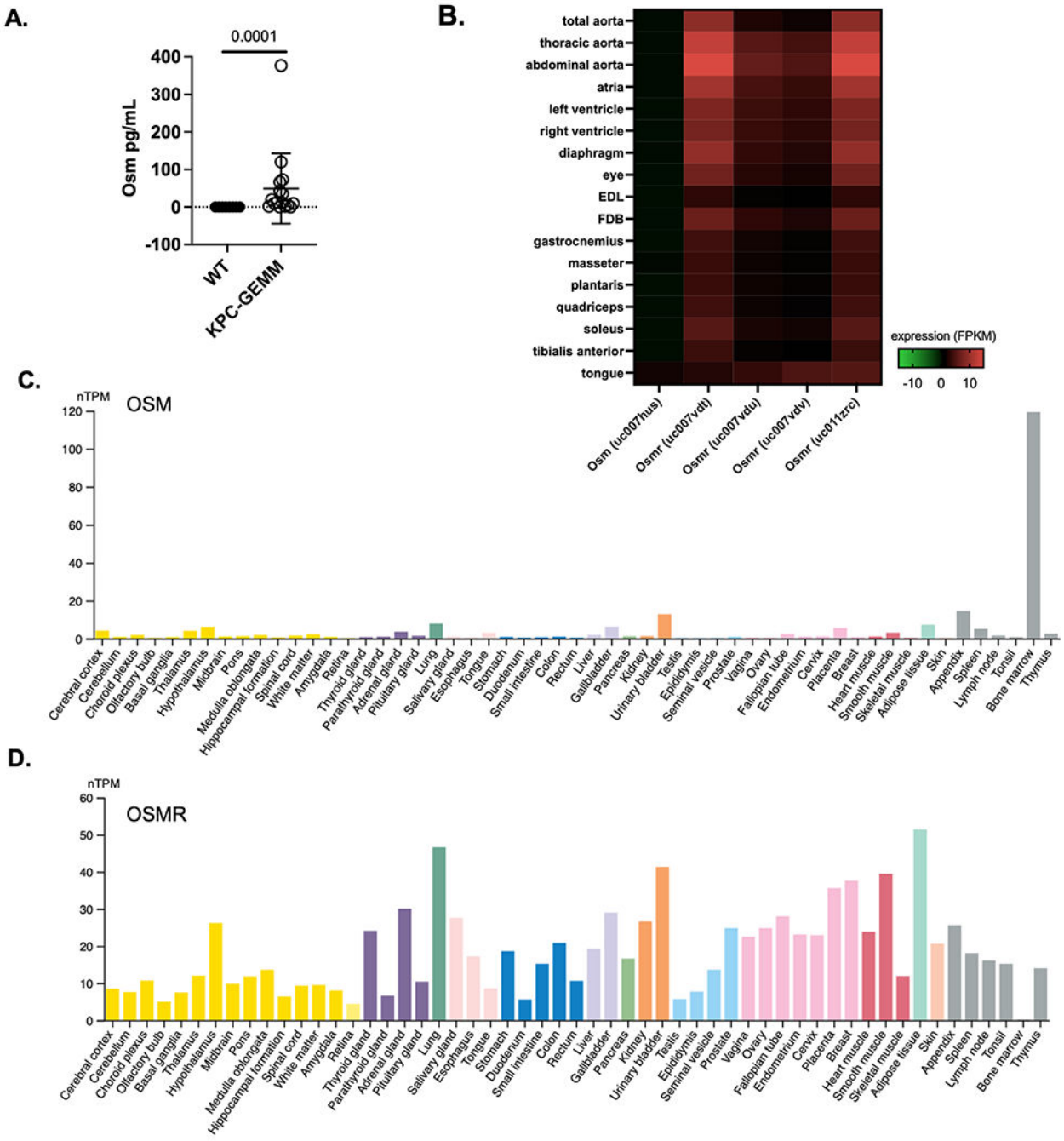

Figure 1. OSM/OSMR expression in normal and cancer cachexia

A. OSM is elevated in plasma in the KPC genetically engineered mouse model (KPC-GEMM) of autochthonic pancreatic cancer. Mann-Whitney test. B. Global mRNA expression of *Osm* and *Osmr* transcripts among normal smooth, cardiac, and skeletal muscle tissues (MuscleDB). B. *OSM* expression is highest in bone marrow, while *OSMR* mRNA is widely expressed across tissues (Human Protein Atlas).

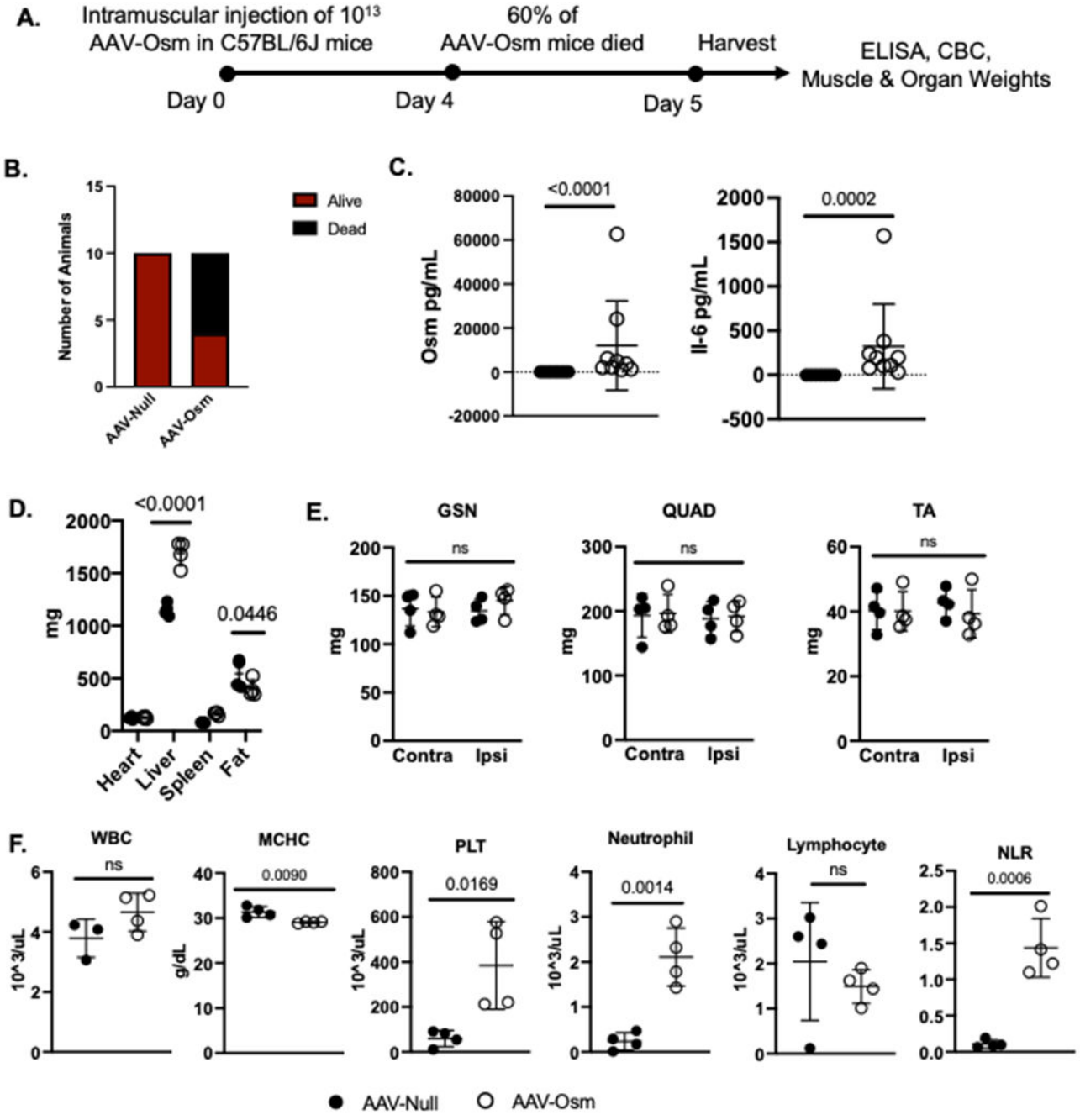

Figure 2. High dose AAV-Osm caused hepatomegaly, adipose loss, and inflammation, but not muscle loss

A. Experimental design. AAV was injected into the right gastrocnemius of wildtype mice. B. High dose AAV-Osm was lethal to mice four days post injection. C. AAV-Osm increased OSM and IL-6 proteins in plasma. D. AAV-Osm induced hepatomegaly and fat loss but exerted no effect on heart and spleen size. E. AAV-Osm did not affect gastrocnemius (GSN), quadriceps (QUAD), or tibialis anterior (TA) muscle mass. F. AAV-OSM showed no statistical difference in white blood cell count (WBC), decreased mean corpuscular

hemoglobin concentration (MCHC), elevated platelets (PLT), and elevated neutrophils, and greatly increased neutrophil/lymphocyte ratio (NLR). Statistical analysis: Unpaired t-test.

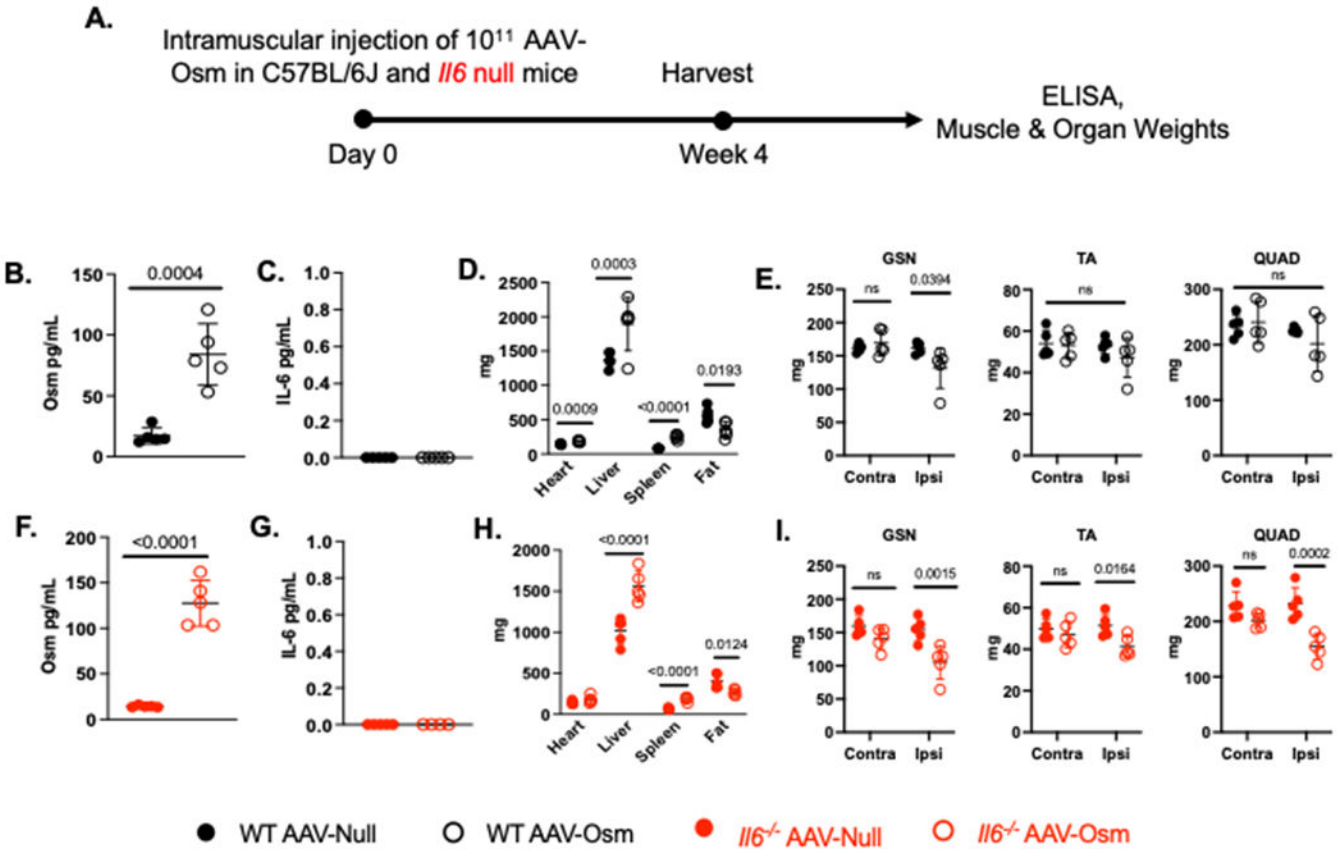

Figure 3. Low dose AAV-Osm causes local muscle and fat loss, and hepato-splenomegaly at 4 weeks

A. Experimental design. AAV was injected into the right gastrocnemius of wildtype mice: AAV-Osm (n=5) and AAV-Null (n=5), and *Il6*$^{-/-}$ mice: AAV-Osm (n=5) and AAV-Null (n=5). The study was conducted for 4 weeks. AAV-Osm elevated OSM levels (B), but not IL-6 levels (C) in wildtype mice. D. AAV-Osm induced cardiac hypertrophy, hepato-splenomegaly, and fat loss in wildtype mice. E. AAV-Osm induced local muscle loss on the ipsilateral side in the gastrocnemius (GSN) in wildtype mice. AAV-Osm elevated OSM levels (F), but not IL-6 levels (G) in *Il6*$^{-/-}$ mice. H. AAV-Osm induced hepato-splenomegaly and fat loss in *Il6*$^{-/-}$ mice. I. AAV-Osm induced muscle loss on the ipsilateral but not contralateral side in the GSN, QUAD, and TA of *Il6*$^{-/-}$ mice. Contralateral (Contra) defines the non-injected side, Ipsilateral (Ipsi) defines the injected side. Statistical Analysis: Two-Way ANOVA with Tukey's Multiple Comparison Test (D-E, H-I) or Unpaired t-test (B-C, F-G).

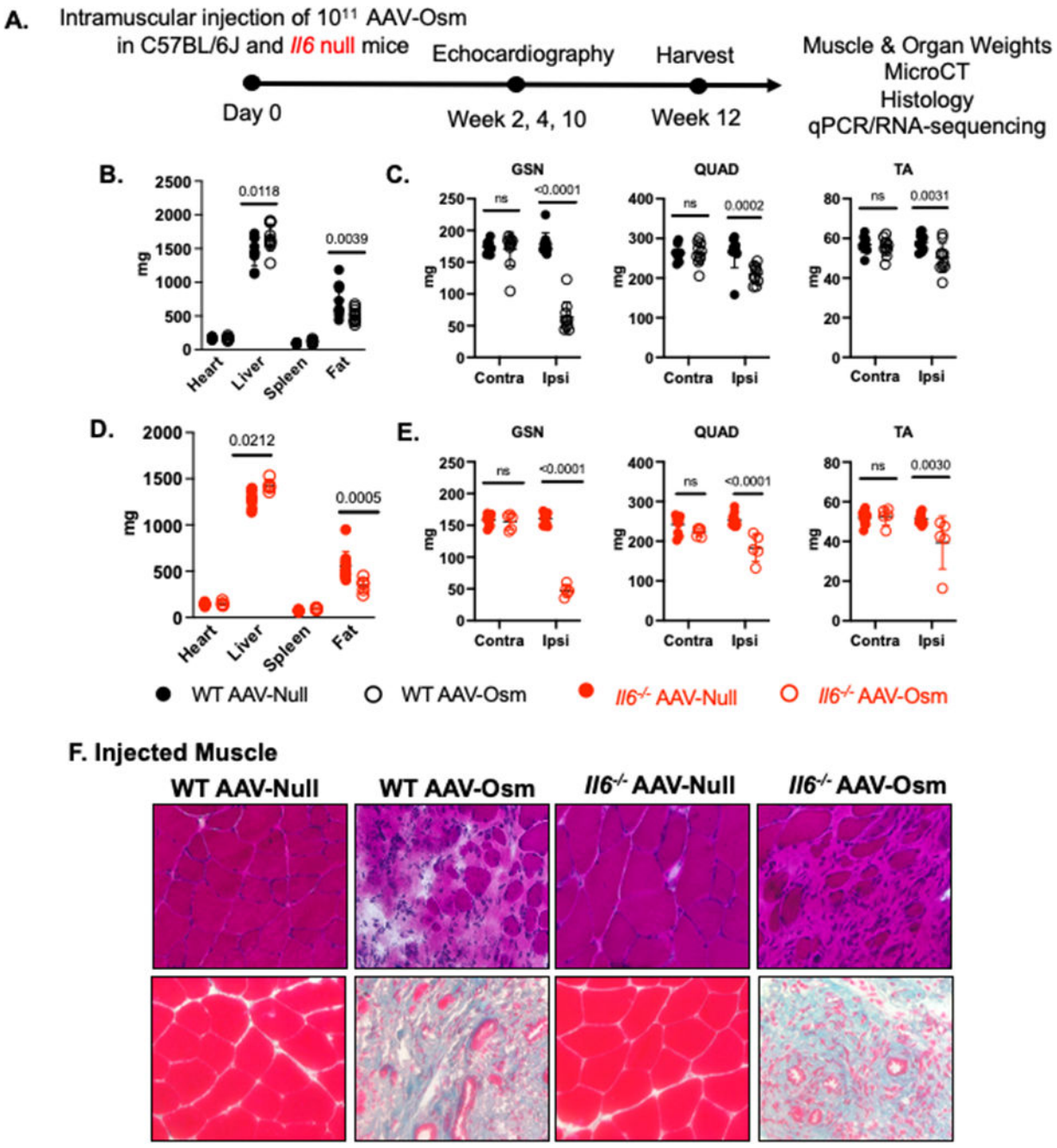

Figure 4. Low Titer AAV-Osm causes local muscle and fat loss, hepatomegaly, and local muscle fibrosis at 12 weeks

A. Experimental design. AAV was injected into the right gastrocnemius of wildtype mice: AAV-Osm (n=10) and AAV-Null (n=10), and *Il6*$^{-/-}$ mice: AAV-Osm (n=10) or AAV-Null (n=10). The study was conducted for 12 weeks. B. AAV-Osm induced hepato-splenomegaly and fat loss in wildtype mice. C. AAV-Osm induced muscle loss in the ipsilateral gastrocnemius (GSN), quadriceps (QUAD), and tibialis anterior (TA) in wildtype mice. D. AAV-Osm induced hepato-splenomegaly and fat loss in *Il6*$^{-/-}$ mice. E. AAV-Osm induced muscle loss on the ipsilateral side in the GSN, QUAD, and TA in *Il6*$^{-/-}$ mice. F. H&E and

Trichrome stains revealed fibrosis and muscle loss in the injected gastrocnemius muscle in AAV-Osm mice but not in AAV-Null. Contralateral (Contra) defines the non-injected side, Ipsilateral (Ipsi) defines the injected side. Statistical Analysis: Two-Way ANOVA with Tukey's Multiple Comparison Test.

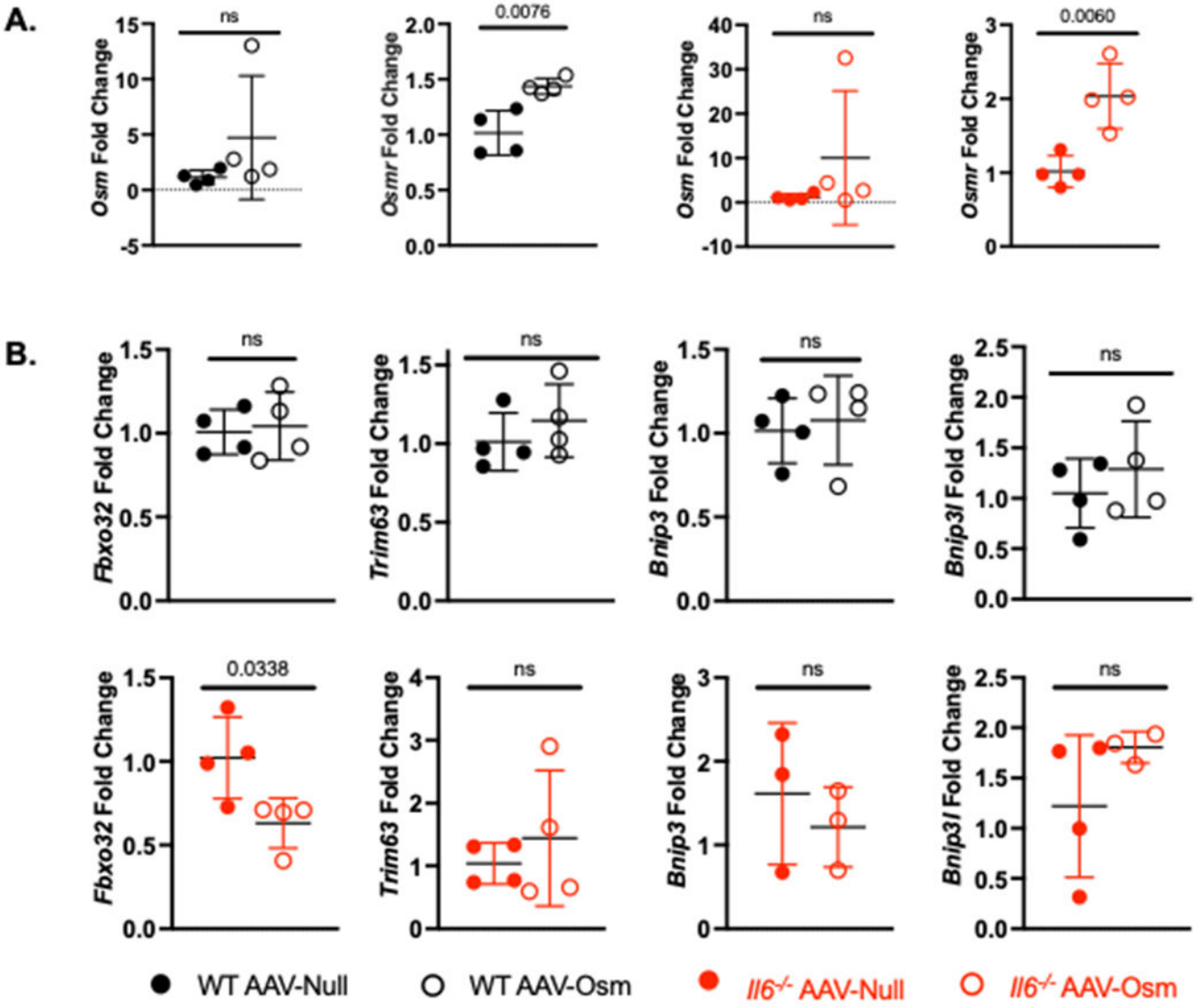

Figure 5. AAV-Osm has minimal effect on gene expression in quadriceps muscle at 12 weeks

A. qPCR results reveal *Osm* was not changed by qPCR in wildtype or *Il6*$^{-/-}$ quadriceps, but *Osmr* expression was elevated in WT and *Il6*$^{-/-}$ quadriceps. B. Atrophy genes *Trim63*, *Bnip3*, and *Bnip3L* were not changed but *Fbxo32* was suppressed in *Il6*$^{-/-}$ quadriceps. Statistical Analysis: Two-Way ANOVA with Tukey's Multiple Comparison Test.

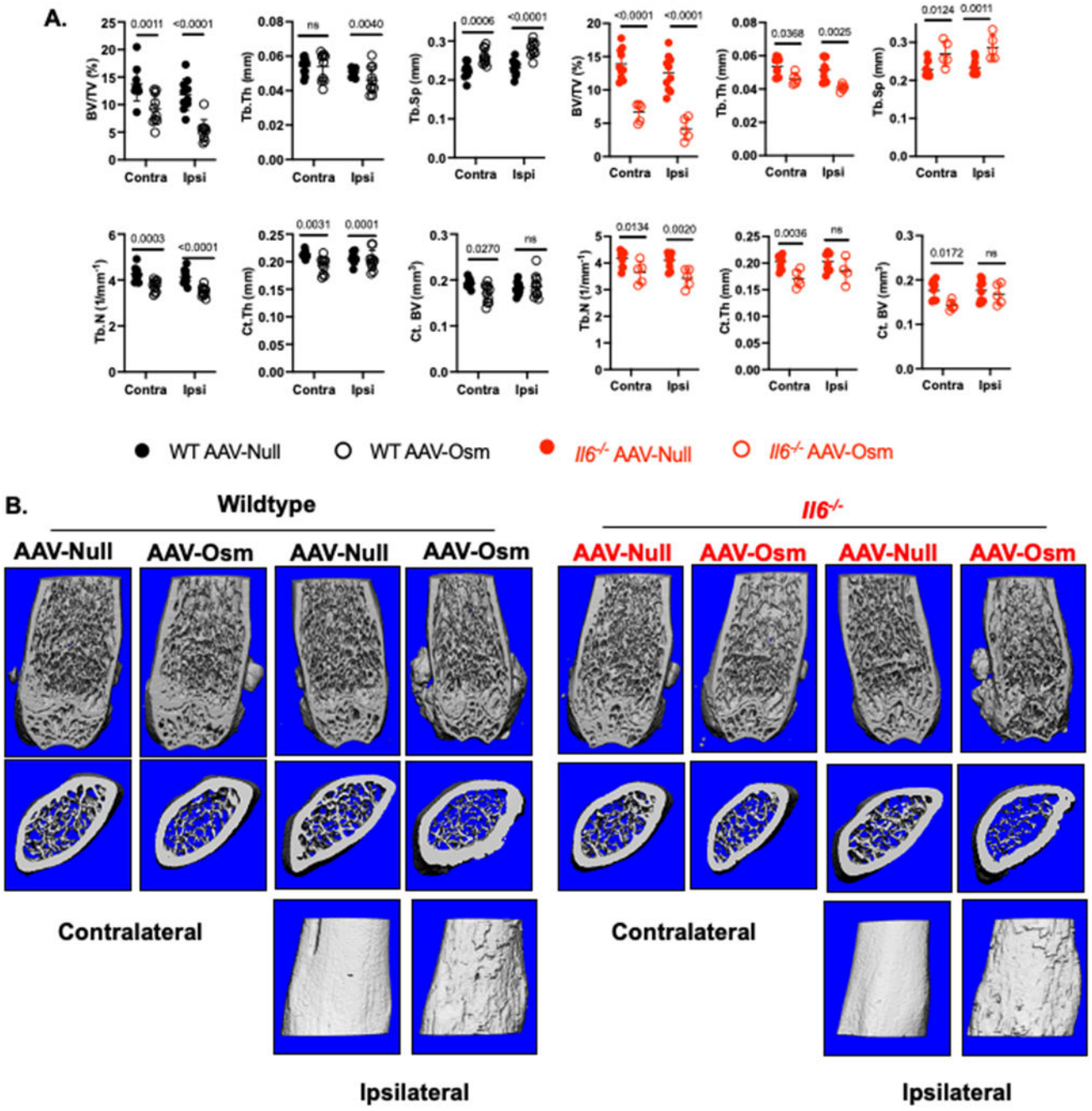

Figure 6. AAV-Osm lowers trabecular bone at 12 weeks

A. AAV-Osm decreased bone volume/total volume (BV/TV%), trabecular thickness (Tb.Th), number (Tb.N) and increased trabecular separation of the (Tb.Sp) in both contralateral and ipsilateral femurs WT and *Il6*$^{-/-}$ mice. AAV-Osm also decreased cortical thickness (Ct.Th) in both femurs and cortical bone volume (Ct.BV) in the contralateral femur of WT mice. AAV-Osm decreased Ct.Th and Ct.BV only in the contralateral femur of *Il6*$^{-/-}$ mice. B. Representative μCT images of contralateral and ipsilateral femurs of WT and *Il6*$^{-/-}$ mice. AAV-Osm induced trabecular island thinning and a woven bone surface phenotype on the

ipsilateral limbs of both genotypes. Contralateral (Contra) defines the non-injected side, Ipsilateral (Ipsi) defines the injected side. Statistical Analysis: Two-Way ANOVA with Tukey's Multiple Comparison Test.

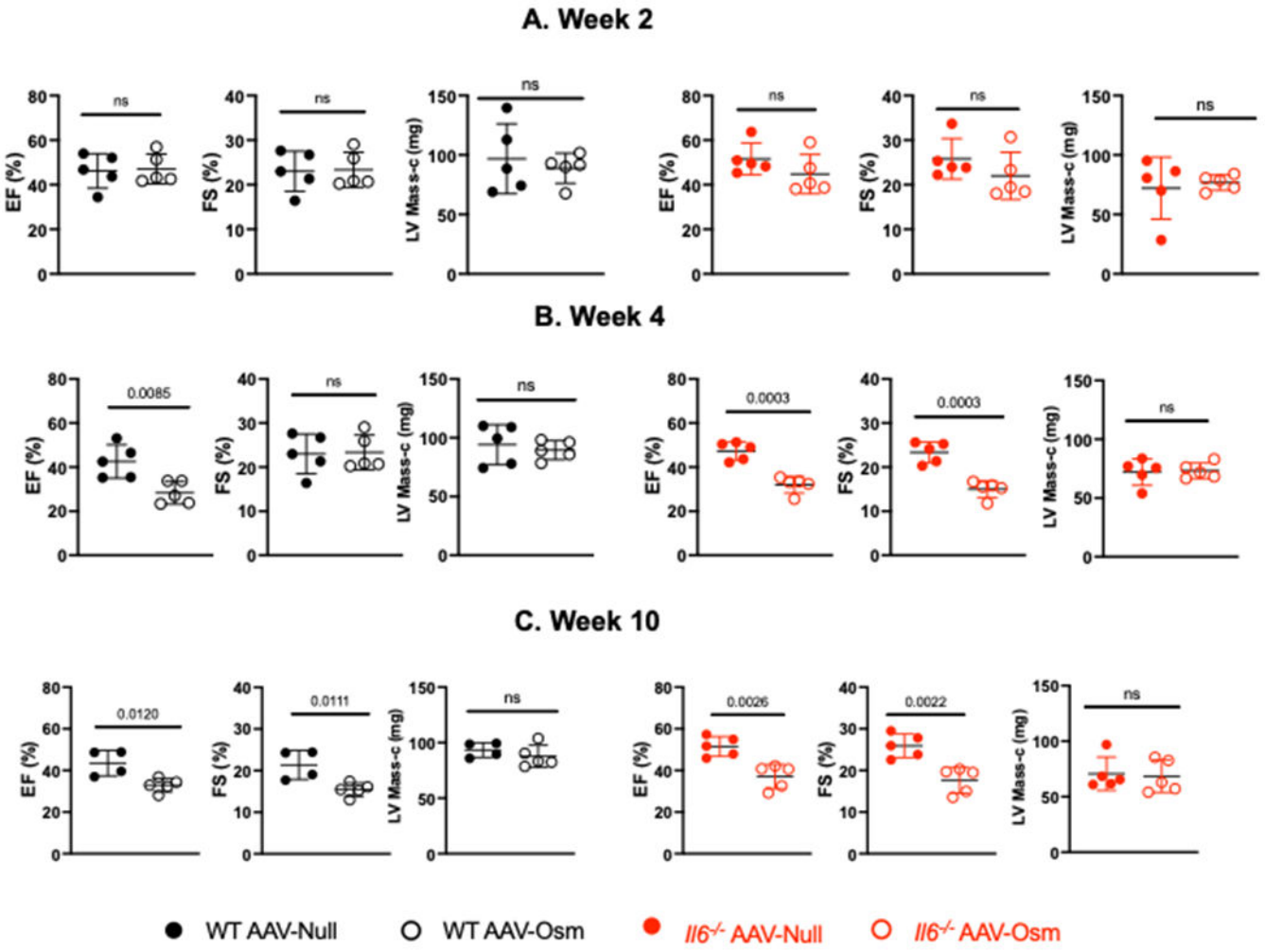

Figure 7. AAV-Osm induces cardiac dysfunction

A. AAV-Osm had no effect on either WT or *Il6*$^{-/-}$ Ejection Fraction% (EF%), Fractional Shortening% (FS%), or LV-mass corrected (LV Mass-c) at week 2. B. By week 4, AAV-Osm reduced EF% and FS% without change to LV-mass. C. AAV-Osm caused sustained cardiac dysfunction in both genotypes, shown by reduced EF% and FS% at week 10. Statistical Analysis: Two-Way ANOVA with Tukey's Multiple Comparison Test.

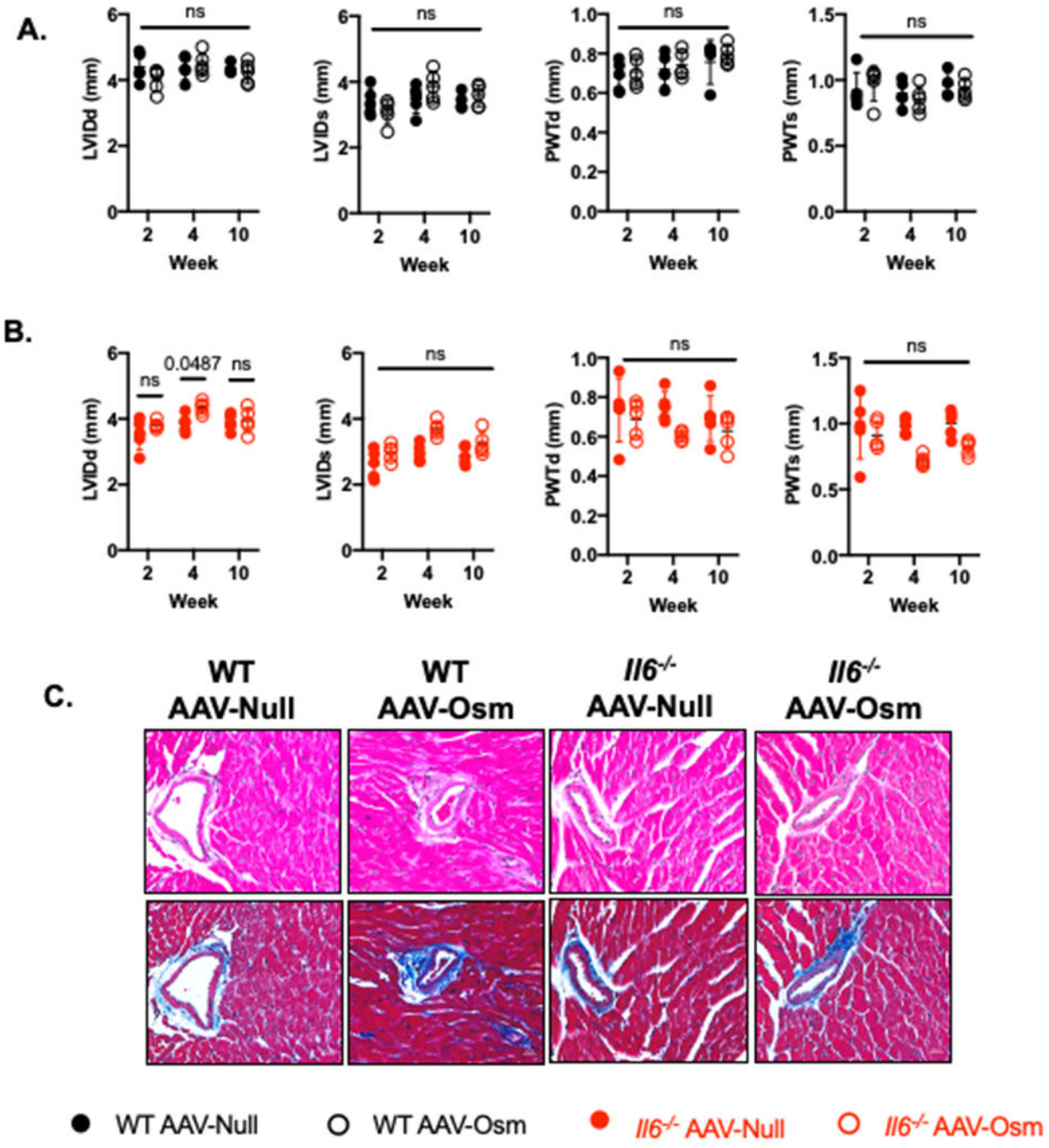

Figure 8. AAV-Osm has minimal effect on cardiac size and fibrosis at 12 weeks

A. In WT mice, AAV-Osm had no effect on left ventricular internal diameter (LVID) or posterior wall thickness (PWT) in diastole (d) or systole (s). B. In *Il6*$^{-/-}$, AAV-Osm had minimal effect on LVID and none on PWT in diastole (d) or systole (s). C. Representative images of H&E and Trichrome of hearts. Statistical Analysis: Two-Way ANOVA with Tukey's Multiple Comparison Test.

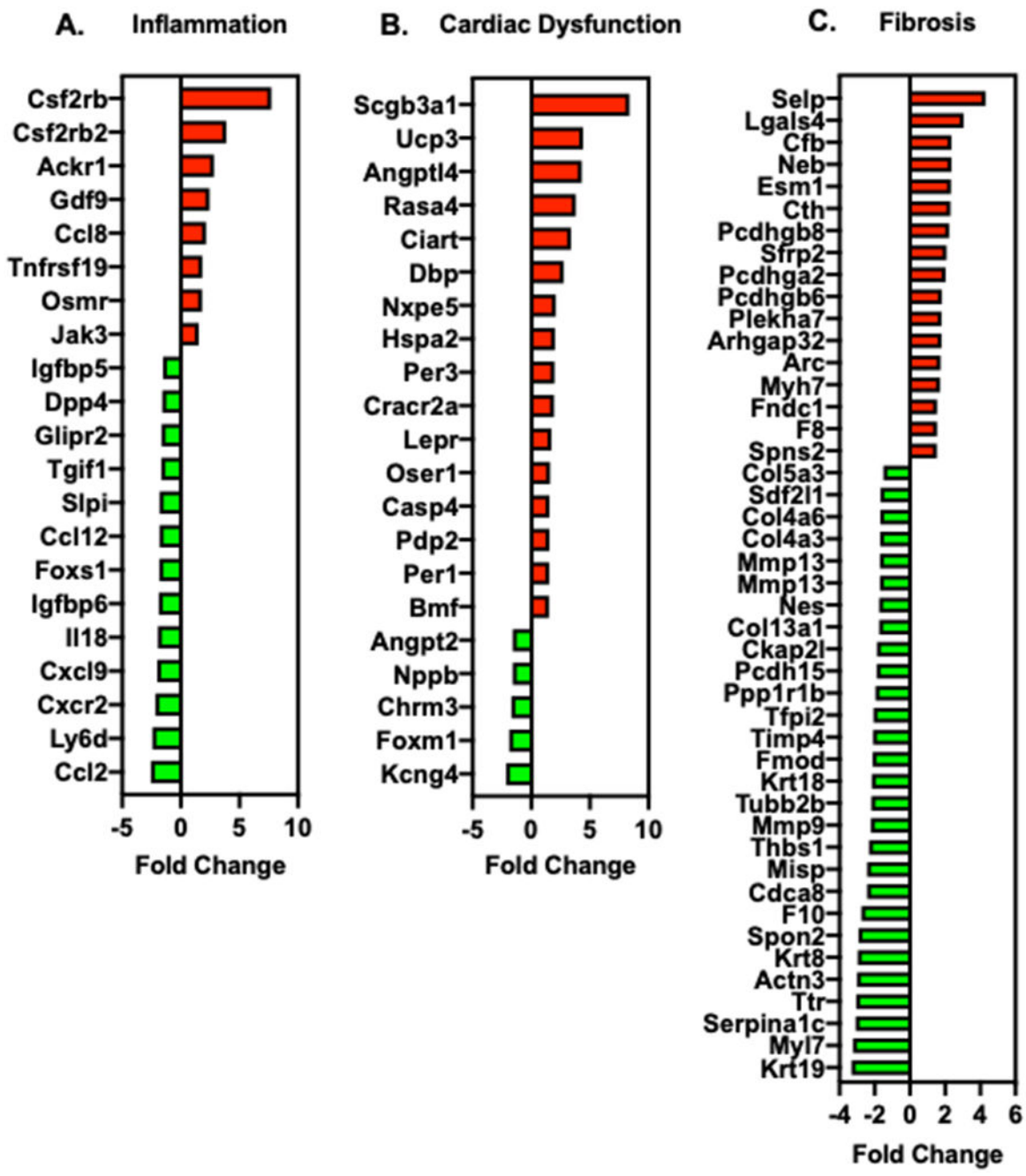

Figure 9. AAV-Osm affects inflammatory, cardiac dysfunction, fibrosis gene expression profiles at 12 weeks

RNA-sequencing results from wildtype cardiac muscle of AAV-Null and AAV-Osm mice. Upregulated (red) and downregulated (green) genes associated with A. Inflammation, B. Cardiac dysfunction, and C. Cardiac fibrosis are shown. Cutoff: $p<0.05$, FC: $|1.5|$.

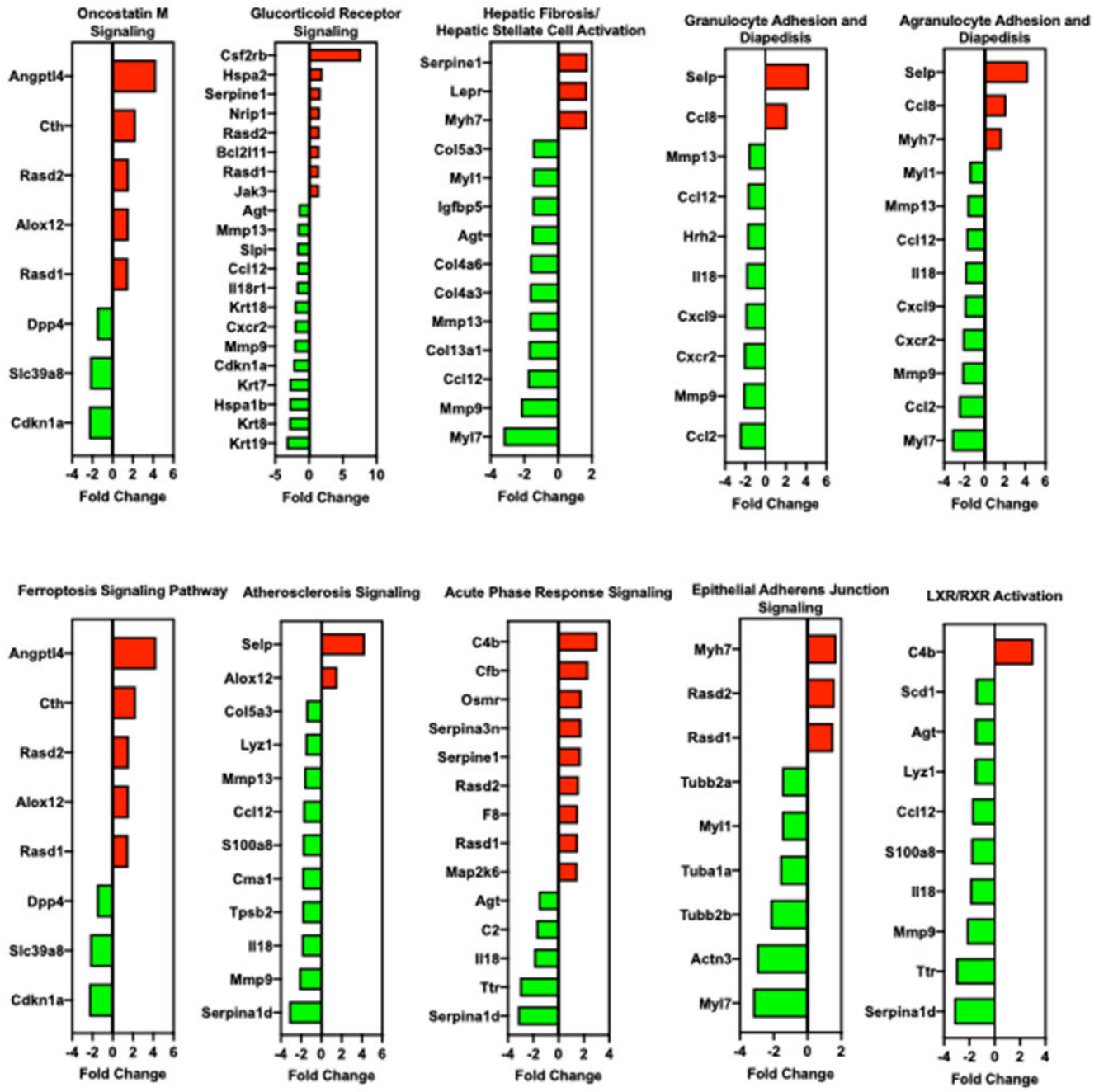

Figure 10. AAV-Osm induces markers of cardiac inflammation at 12 weeks

RNA-sequencing results from wildtype cardiac muscle of AAV-Null and AAV-Osm mice. Ingenuity Pathway Analysis reveals the top 10 canonical pathways. Genes upregulated (red) and downregulated (green). Cutoff: $p<0.05$, fold-change |1.5|.

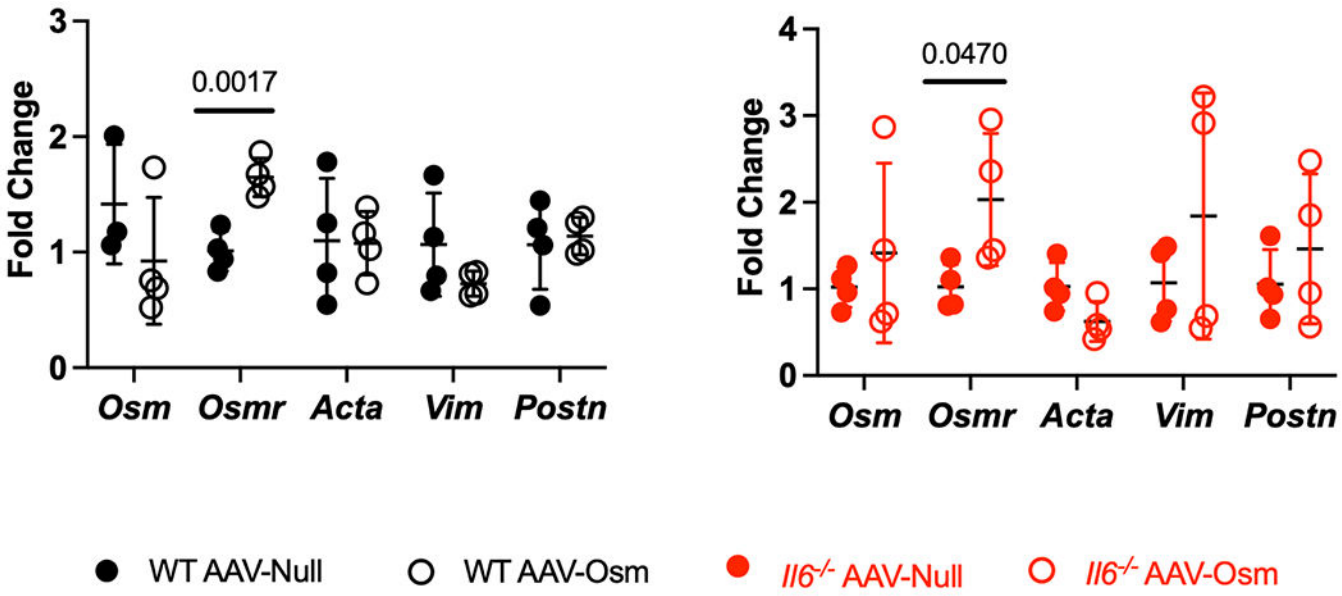

Figure 11. AAV-Osm induces Osmr expression in *Il6*$^{-/-}$ cardiac muscle at 12 weeks

qPCR of WT and *Il6*$^{-/-}$ cardiac muscle from AAV-Null and AAV-Osm mice reveal AAV-Osm increased expression of *Osmr* in both genotypes without change in *Osm*, smooth muscle actin (*Acta2*), vimentin (*Vim*), or periostin (*Postn*). Statistical analysis: Unpaired t-test.

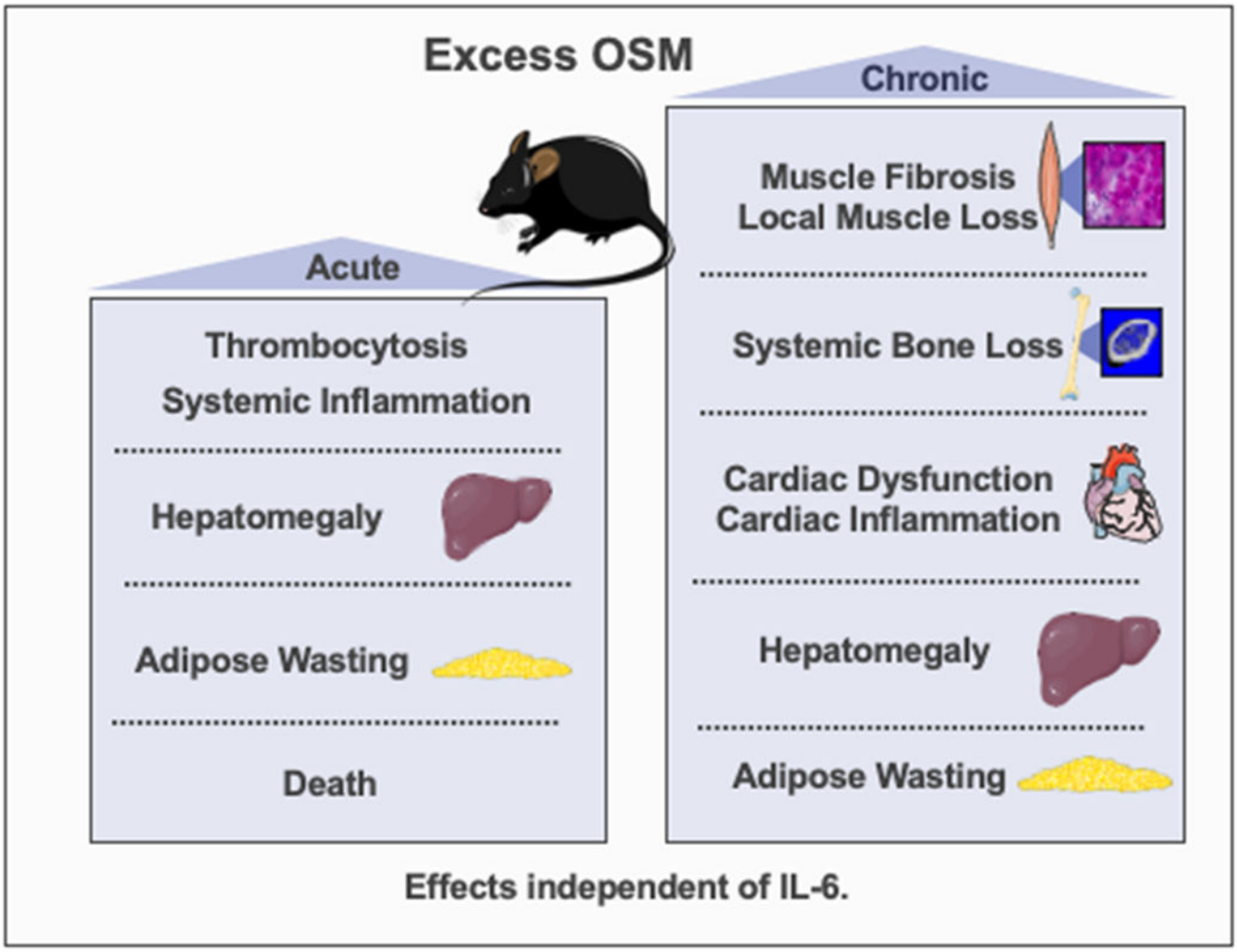

Figure 12. Systemic effects of OSM

Acute exposure of high dose OSM induced thrombocytosis, systemic inflammation, hepatomegaly, adipose wasting, and lethality in wildtype mice. Chronic exposure of low dose OSM in wildtype and IL-6 null mice induced muscle fibrosis and local muscle loss, systemic bone loss, cardiac dysfunction and cardiac inflammation, hepatomegaly, and adipose wasting. These effects were independent of IL-6.

Table 1.

Primers.

Application	Primer Name	Assay ID (Thermo Fisher Scientific)	Amplicon length (bp)
qRT-PCR	Osm	Mm01193966_m1	82
	Osmr	Mm01307326_m1	84
	Bnip3	Mm01275600_g1	147
	Bnip3-L	Mm00786306_s1	141
	Trim63	Mm01185221_m1	57
	Fbxo32	Mm00499523_m1	73
	Tbp	Mm00446974_m1	105
	Postn	Mm01284919_m1	62
	Vim	Mm01333430_m1	62
	Acta2	Mm00725412_s1	95